J Mol Model (2011) 17:2337–2352
DOI 10.1007/s00894-011-1023-6

ORIGINAL PAPER

Applications of the ETS-NOCV method in descriptions of chemical reactions

Mariusz Paweł Mitoraj · Monika Parafiniuk · Monika Srebro · Michał Handzlik · Agnieszka Buczek · Artur Michalak

Received: 11 October 2010 / Accepted: 16 February 2011 / Published online: 29 March 2011

Abstract The present study characterizes changes in the electronic structure of reactants during chemical reactions based on the combined charge and energy decomposition scheme, ETS-NOCV (extended transition state–natural orbitals for chemical valence). Decomposition of the activation barrier, $\Delta E^{\#}$, into stabilizing (orbital interaction, ΔE_{orb}, and electrostatic, ΔE_{elstat}) and destabilizing (Pauli repulsion, ΔE_{Pauli}, and geometry distortion energy, ΔE_{dist}) factors is discussed in detail for the following reactions: (**I**) hydrogen cyanide to hydrogen isocyanide, HCN→CNH isomerization; (**II**) Diels-Alder cycloaddition of ethene to 1,3-butadiene; and two catalytic processes, i.e., (**III**) insertion of ethylene into the metal-alkyl bond using half-titanocene with phenyl-phenoxy ligand catalyst; and (**IV**) B–H bond activation catalyzed by an Ir-containing catalyst. Various reference states for fragments were applied in ETS-NOCV analysis. We found that NOCV-based deformation densities ($\Delta\rho_i$) and the corresponding energies $\Delta E_{orb}(i)$ obtained from the ETS-NOCV scheme provide a very useful picture, both qualitatively and quantitatively, of electronic density reorganization along the considered reaction pathways. Decomposition of the barrier $\Delta E^{\#}$ into stabilizing and destabilizing contributions allowed us to conclude that the main factor responsible for the existence of positive values of $\Delta E^{\#}$ for all processes (**I**, **II**, **III** and **IV**) is Pauli interaction, which is the origin of steric repulsion. In addition, in the case of reactions **II**, **III** and **IV**, a significant degree of structural deformation of the reactants, as measured by the geometry distortion energy, plays an important role. Depending on the reaction type, stabilization of the transition state (relatively to the reactants) originating either from the orbital interaction term or from electrostatic attraction can be of vital importance. Finally, use of the ETS-NOCV method to describe catalytic reactions allows extraction of information on the role of catalysts in determination of $\Delta E^{\#}$.

Keywords ETS-NOCV scheme · Chemical reaction · Deformation density · Chemical bonding · Reference state

Electronic supplementary material The online version of this article (doi:10.1007/s00894-011-1023-6) contains supplementary material, which is available to authorized users.

M. P. Mitoraj (✉) · M. Parafiniuk · M. Srebro · M. Handzlik · A. Buczek · A. Michalak
Department of Theoretical Chemistry, Faculty of Chemistry, Jagiellonian University,
R. Ingardena 3,
30–060, Krakow, Poland
e-mail: mitoraj@chemia.uj.edu.pl

Introduction

One of the most important goals of theoretical chemistry is to characterize and predict the reactivity of molecular systems [1, 2]. In order to achieve this goal, many methods suited to the description of electronic structure can be applied. Such methods include, for instance, molecular orbitals (MOs) [3, 4], localized molecular orbitals (LMOs) [5–7], bond orders [8–17], atoms in molecules (AIM) theory [18], Fermi hole-based concepts [19], and various charge and energy decomposition schemes [20–25]. A useful and elegant approach based on the reaction force concept and suitable for description of energy profiles of chemical reactions was proposed by Torro-Labbe and co-workers [26]. Very recently, Bickelhaupt and Zeist proposed the so-called "activation strain model", which also appeared to be useful in the analysis of chemical reactions [27].

We have recently developed the ETS-NOCV scheme [28–32] by combining the extended transition state (ETS) [22, 23] energy decomposition approach with the natural orbitals for chemical valence (NOCV) method [33–38]. It was shown that ETS-NOCV is suitable for a qualitative and quantitative description of the crucial components (σ, π, δ, etc.) that constitute various types of chemical bonds, including donor–acceptor [28, 30, 31, 33, 34, 37, 38], covalent [28, 35], and weak intra- [28, 29] and intermolecular interactions [32]. Thus, ETS-NOCV offers a compact characterization of chemical bonds. However, only structures that correspond to minima on the potential energy surface (PES) have been studied up to now.

Therefore, the main goal of this article was to apply the ETS-NOCV approach, for the first time, to analysis of changes in the electronic structure of reactants along reaction paths. We first consider two simple, model reactions: (**I**) hydrogen cyanide to hydrogen isocyanide, HCN→CNH, isomerization; and (**II**) Diels-Alder cycloaddition of ethene to 1,3-butadiene (see Fig. 1) [39, 40]. Afterwards, we will discuss briefly one of the elementary reactions occurring in the ethylene polymerization cycle catalyzed by organometallic complexes, namely insertion of the monomer into the metal-alkyl bond proceeding via the backside propagation mechanism (see reaction **III** in Fig. 1) [41, 42]. In this example, a half-titanocene complex with the cyclopentadienide Cp* and 2-phenyl-phenoxy ligand combination was considered as the catalyst. Its high catalytic performance in the ethylene polymerization processes has been thoroughly studied recently [43–45].

Finally, we will perform a theoretical study on the selective activation of the B–H bond of ammonia borane (NH_3BH_3, abbreviated as AB) catalyzed by an Ir-containing catalyst (see reaction **IV** in Fig. 1) [46]. The results on the factors determining the barrier to activation of the B–H bond of AB could, in addition, be useful in the rational design of new catalysts suitable for effective dehydrogenation of AB since it is considered an efficient hydrogen storage medium [47].

We will use the ETS-NOCV method to analyze the electronic structure at characteristic points on the PES [substrate (S), transition state (TS), and product (P), see Fig. 1]. Decomposition of the activation barrier (for reactions **I**– **IV**) into stabilizing (electronic and electrostatic) and destabilizing (Pauli repulsion and distortion energy) factors will be discussed in detail (S→TS step of the reaction).

Theoretical background

Our analysis is based on the ETS-NOCV approach, which is a combination of the extended transition state (ETS) energy decomposition analysis [22, 23] with the natural orbitals for chemical valence (NOCV) scheme [33–38].

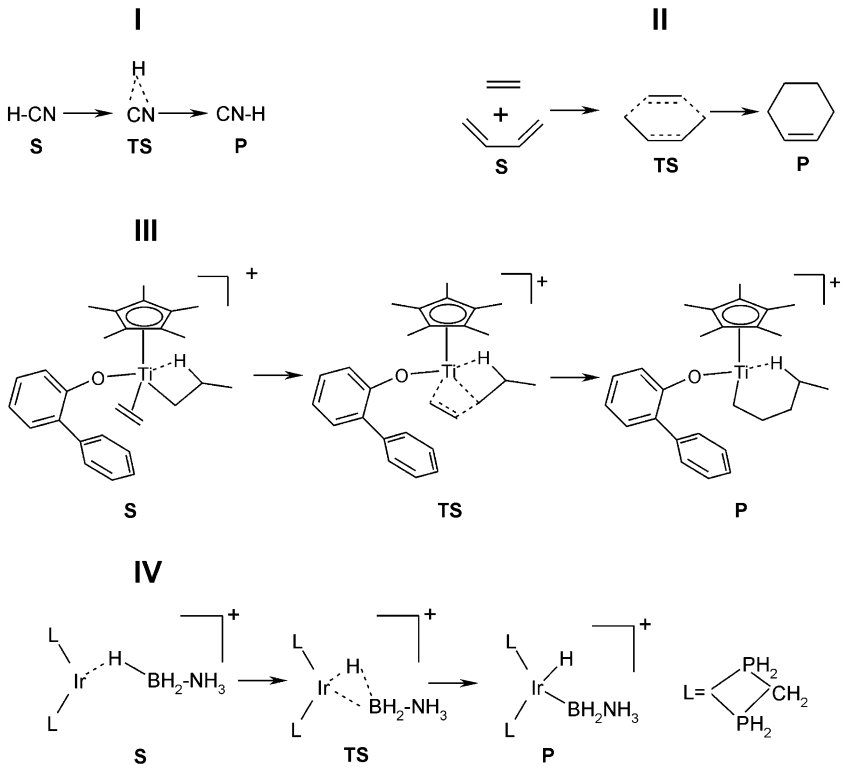

Fig. 1 Reactions studied in this article

Extended transition state method

In the original ETS scheme, the total bonding energy between the interacting fragments (ΔE_{total}) is divided into four chemically meaningful components, Eq. 1:

$$\Delta E_{\text{total}} = \Delta E_{\text{dist}} + \Delta E_{\text{elstat}} + \Delta E_{\text{Pauli}} + \Delta E_{\text{orb}} \quad (1)$$

The first component, referred to as the distortion term ΔE_{dist}, represents the amount of energy required to promote the separated fragments from their equilibrium geometry to the structure they will take up in the combined molecule. The second term, ΔE_{elstat}, corresponds to the classical electrostatic interaction between the promoted fragments as they are brought to their positions in the final complex. The third term, ΔE_{Pauli}, accounts for the repulsive Pauli interaction between occupied orbitals on the two fragments in the combined complex. Finally, the last term, ΔE_{orb}, represents the stabilizing interactions between the occupied molecular orbitals on one fragment with the unoccupied molecular orbitals of the other fragment, as well as the mixing of occupied and virtual orbitals within the same fragment (intra-fragment polarization) after the two fragments have been united. We can write the change in density that gives rise to ΔE_{orb} as

$$\Delta\rho(1) = \sum_{\lambda}\sum_{\nu} \Delta P_{\mu\nu}\lambda(1)\nu(1) \quad (2)$$

where the sum is over all the occupied and virtual molecular orbitals on the considered fragments. It now follows from the ETS scheme that the ΔE_{orb} term [22, 23] is given by

$$\Delta E_{orb} = \sum\nolimits_{\lambda}\sum\nolimits_{\mu} \Delta P_{\lambda\mu}F^{T}_{\lambda\mu} \quad (3)$$

where $F^{TS}_{\lambda\mu}$ is a Kohn-Sham Fock matrix element that is defined in terms of a "transition state" potential that is midway between that of the combined fragments and the final molecule, hence the term transition state.

Natural orbitals for chemical valence

Turning next to the NOCV approach, we note that the NOCV [33–38] are derived from Nalewajski-Mrozek valence theory [11–17]. However, from a mathematical point of view, the NOCVs, ψ_i, are simply defined as the eigenvectors,

$$\psi_i(1) = \sum_{\lambda}^{M} C_{i,\lambda}\,\lambda(1) \quad (4)$$

that diagonalize the deformation density matrix ΔP introduced in Eq. 2. Thus,

$$\Delta P C_i = v_i C_i \quad ; \quad i{=}1,M \quad (5)$$

where M denotes the total number of molecular orbitals on the fragments and C_i is a column vector containing the coefficients that defines the NOCV ψ_i of Eq. 4. It follows further [28–38] that the deformation density $\Delta\rho$ of Eq. 2 can be expressed in the NOCV representation as a sum of pairs of complementary eigenfunctions (ψ_{-k} , ψ_k) corresponding to the eigenvalues $-v_k$ and $+v_k$ with the same absolute value but opposite signs:

$$\Delta\rho(r) = \sum_{k=1}^{M/2} v_k\left[-\psi^2_{-k}(r) + \psi^2_k(r)\right] = \sum_{k=1}^{M/2} \Delta\rho_k(r) \quad (6)$$

Expression 6 is the most important for the interpretation of NOCV, as it defines the charge-flow channels decomposing the overall deformation density. Therefore, in the present study, we will not discuss the orbitals themselves, but only the respective deformation density contributions, $\Delta\rho_k$. Examples of NOCVs and their interpretation can be found elsewhere [33].

ETS-NOCV analysis

In the combined ETS-NOCV scheme [28–32], the orbital interaction component (ΔE_{orb}) is expressed in terms of NOCVs as

$$\Delta E_{orb} = \sum_{k} \Delta E_{orb}(k) = \sum_{k=1}^{M/2} v_k\left[-F^{TS}_{-k,-k} + F^{TS}_{k,k}\right] \quad (7)$$

where $F^{TS}_{-k,-k}$ and $F^{TS}_{k,k}$ are diagonal Kohn-Sham matrix elements defined over NOCVs with respect to the TS density. The advantage of the expression in Eq. 7 for ΔE_{orb} over that of Eq. 3 is that only a few complementary NOCV pairs normally contribute significantly to ΔE_{orb}. It is clear from Eqs. 6, and 7 that, for each complementary NOCV pair representing one of the charge transfer channel $\Delta\rho_k$, we not only can depict $\Delta\rho_k$ but also provide the energy contributions $\Delta E_{orb}(k)$ to the bond energy from $\Delta\rho_k$ [28–32].

Chemical reactions and ETS-NOCV analysis—arbitrariness of the reference state

It should be emphasized strongly that the ETS-NOCV approach provides a way to decompose the deformation density (differential density) corresponding to the formation of the whole molecular system *from the considered molecular fragments* and the corresponding energy of the interaction *between these fragments*. Thus, this analysis has some inherent arbitrariness, which is in fact present in all methods referring to the concepts of bonds in molecules and atoms in molecules [48], that are not defined strictly by physical observables.

In many cases, when discussing various bonds in stable molecular systems (minima on the respective PES), the choice of fragments is quite intuitive and natural, e.g., by separating a functional group or a ligand from the remaining part of the considered system. However, the arbitrariness of the choice of reference fragments may become a serious difficulty when discussing changes in the electronic structure along a pathway of a given chemical reaction. This is because, in many cases, fragments that arise as a 'natural' choice for a description of the initial reactant stage, are not so intuitive for the TS or the product of the reaction. Let us consider, for instance, the simple cycloaddition Diels-Alder reaction: ethylene+butadiene→ cyclobutene. When considering initial stages of this reaction with weakly interacting reactants, a division of the reactive system into two fragments, ethylene and butadiene, both in the close shell ground states, is quite intuitive. In a description of the bonding between those fragments in the product cyclobutene, however, the question arises whether the ethylenic and butadienic fragments in the triplet states should be considered instead as more relevant, since two single bonds are broken by such a fragmentation. And what about the TS region? In a general case, both singlet and triplet fragments seem to be arbitrary here, unless the TS is clearly reactant-like (early TS) or product-like (late TS).

Therefore, it can be expected that, in many cases, the chemical reaction analyzed in terms of molecular fragments can be discussed *from the reactant(s) perspective* or *from the product(s) perspective*. In a general case, these two perspectives may provide two different views, often complementary but at the same time 'discontinuous'. In the present account, we will discuss this point in more detail, based on the example results obtained for the cycloaddition reaction using both the reactant perspective and the product perspective.

Furthermore, in addition to alternative electronic states of the reference fragments, in the case of some reactions it may be valuable to consider alternative number of electrons on the fragments (charged species vs neutral species). For example, in the case of the HCN→CNH isomerization reaction analyzed here, one can consider the ionic, closed-shell fragments, H^+ and CN^-, as a natural alternative to the neutral radicals, $H^{\cdot}$ and $CN^{\cdot}$. Such a ionic reference frame will be as well discussed for the isomerization reaction.

Computational details

All the DFT calculations presented here were based on the Amsterdam density functional (ADF 2009.01) program [49–53] in which the ETS-NOCV scheme was implemented [28–32]. The Becke-Perdew exchange-correlation functional [54, 55] was applied (BP86). A standard triple-zeta STO basis containing one set of polarization functions (TZP) was adopted for metal atoms, Ti and Ir, whereas for the remaining elements (H, B, C, N, and O), standard double-zeta STO with one set of polarization functions (DZP) were considered. The 1s electrons of C, N, O, B, 1s-2p electrons of Ti, as well as the 1s-3d electrons of Ir were treated as a frozen core. The contours of deformation densities were plotted based on the ADF-GUI interface [56]. Relativistic effects for atoms involved in reaction **IV** were included at the ZORA level of approximation as implemented in ADF 2009.01 program [57–59].

In ETS-NOCV analysis of reaction **I**, we considered primarily the interaction between two radicals in doublet spin state H↑ and CN↓ at S, TS and P. Further, this reaction was also analyzed using the charged species H^+ and CN^- as the reference state.

In the case of reaction **II**, the two closed shell ethene and 1,3-butadiene were predominantly chosen—so called reactant perspective. For comparison, we also described reaction **II** from the product perspective, i.e., triplet fragments were considered.

Fragments of ethene and Ti-containing catalyst in the singlet spin states were predominantly applied for **III-S** and **III-TS**. We believe that the singlet spin state for fragments in **II-TS** and **III-TS** is a reasonable choice due to the "early" character of the TS, i.e., minor changes in geometry are observed when going from the reactants to the TS (see the scheme S1 in the electronic supplementary material). In the case of the products **II-P** and **III-P**, the triplet spin states for fragments were predominantly used.

Finally, in the case of reaction **IV**, the interaction between three fragments was analyzed primarily (H↑, NH_3H_2B↓ and closed shell Ir-catalyst) at both points on the PES, **IV-S** and **IV-TS**. Again, we kept the same spin state for fragments in **IV-S** and **IV-TS** due to the "early" character of **IV-TS**. For the product, however, we used predominantly radical fragments H↑, NH_3H_2B↓ and the triplet state of the Ir-catalyst (↑↑). We have chosen the "three-fragment resolution" approach in order to gain insight into the breaking of the B–H bond and formation of the new Ir–H and Ir–B connections during the course of activation. In addition, for comparison, we have also performed ETS-NOCV analysis by applying (1) two closed shell fragments (NH_3BH_3 and Ir-containing catalyst), and (2) charged closed shell fragments (H^+, $NH_3H_2B^-$ and Ir-catalyst).

Results and discussion

Reaction I: HCN→CNH isomerization

Let us first discuss the changes in electronic structure during the hydrogen cyanide to hydrogen isocyanide isomerization, H–CN→CN–H, using two radicals, H↑ and

CN↓, in the doublet spin state as a reference. Throughout the manuscript, the labeling of reactants outlined in Fig. 1 will be used. It is evident from the data presented in the first part of Table 1 (referring to radical fragments) that the electronic factor, i.e., orbital interaction term, ΔE_{orb}, becomes systematically more stabilizing when going from **I-S** (ΔE_{orb}=−176.4 kcal mol^{-1}) through **I-TS** (ΔE_{orb}= −222.1 kcal mol^{-1}) to **I-P** (ΔE_{orb}=−240.7 kcal mol^{-1}).

To shed light on the qualitative charge rearrangements on the isomerization pathway, and to rationalize the trend in ΔE_{orb} values, Fig. 2b presents the dominant deformation density contribution, $\Delta\rho_1$, with the corresponding energy, $\Delta E_{orb}(1)$. It is clear that $\Delta\rho_1$ for **I-S** represents formation of the H–C bond and lone electron pair on the nitrogen atom. In addition, an accumulation of electrons in the CN bonding region is observed. The $\Delta\rho_1$ electron transfer corresponds to the total electronic stabilization, $\Delta E_{orb}(1)$=−158.3 kcal mol^{-1}. It should be noted that the remaining $\Delta\rho$ contributions correspond to the intra-fragment polarization within the CN radical, and they barely contribute to H–CN bonding.

In the transition state, **I-TS**, $\Delta E_{orb}(1)$ further decreases (becomes more stabilizing), reaching a value of −196.8 kcal mol^{-1}. It can be concluded from the contour of $\Delta\rho_1$ that in **I-TS**, apart from the H–C bond already present, a new N–H connection is formed, which is represented by the accumulation of the electron density in both HC and NH regions. The presence of such two bonds leads to increased electronic stabilization of **I-TS** as compared to **I-S**.

Finally, the product of isomerization, **I-P**, $\Delta\rho_1$ captures both formation of N–H bond and lone electron pair on carbon atom, and accumulation of electrons in the C≡N bonding region. This corresponds to the largest stabilization, $\Delta E_{orb}(1)$= −204.3 kcal mol^{-1}. Thus, a systematic drop (increasing stabilization) in the total orbital interaction term, ΔE_{orb}, is related to a decrease in the $\Delta E_{orb}(1)$ values on the isomerization pathway.

It is worth noting that the systematic increase in the orbital-interaction stabilization in the order S,TS, P indicates an increase in ionicity of the H–(CN) bond, since the component describes the net H→(CN) electron transfer (from one-electron H$^{\cdot}$ radical to CN$^{\cdot}$ radical towards formation $H^{\delta+}CN^{\delta-}$ with increasing δ). This picture emerging from the ETS-NOCV approach is fully consistent with the corresponding increase in the Hirshfeld and Vornoi atomic charge on the hydrogen atom, as shown in the bottom part of Table 1, $q_H(S)<q_H(TS)<q_H(P)$.

Let us now discuss the remaining contributions to the bonding energy. It is important to note that the same stabilizing trend as for ΔE_{orb}, although quantitatively less pronounced, is observed in the case of electrostatic stabilization, ΔE_{elstat}**(I-TS)**−ΔE_{elstat}**(I-S)**=−31.1 kcal mol^{-1}. This is a consequence of increased inter-penetration of the density on the hydrogen atom and the density of the CN unit.

On the one hand, the conformation of TS with two H–C and H–N bonding interactions leads to the stabilization of **I-TS** due to orbital and electrostatic factors; however, at the same time it causes very strong destabilization originating from the Pauli repulsion term, ΔE_{Pauli}**(I-TS)**−ΔE_{Pauli}**(I-S)**=122.2 kcal mol^{-1}. Such a destabilization, resulting predominantly from the repulsive interaction of the electron on the hydrogen with occupied σ(CN) and two π(CN) orbitals, overcompensates for the total stabilization stemming from both ΔE_{orb} and ΔE_{elstat} values. Accordingly, the barrier of the isomerization appears, and is $\Delta E^{\#}=\Delta E_{total}$**(I-TS)**−$\Delta E_{total}$**(I-S)**=45.5 kcal mol^{-1}, see Fig. 2a and Table 1. The contribution to $\Delta E^{\#}$ coming from

Table 1 Extended transition state (ETS)[a] energy decomposition results (in kcal mol^{-1}) describing the bond between hydrogen and CN radicals for reaction **I** substrate (S), transition state (TS), and product (P) (**I-S**, **I-TS**, **I-P**) together with the corresponding Hirshfeld and Vornoi charges on hydrogen atoms. Charged species H^+ and CN^- were also considered in ETS analysis

ETS results / H charges	H-CN I-S	TS I-TS	CN-H I-P	$\Delta E^{\#}$ [(I-TS)-(I-S)]
Radical fragments:				
ΔE_{total}[b]	-133.3	-87.8	-118.6	45.5
ΔE_{orb}	-176.4	-222.1	-240.7	-45.7
ΔE_{Pauli}	91.6	213.8	194.7	122.2
ΔE_{elstat}	-48.7	-79.8	-72.6	-31.1
ΔE_{dist}	0.3	0.4	0.0	0.1
Charged fragments:				
ΔE_{total}[c]	-357.4	-311.9	-342.6	45.5
ΔE_{orb}	-179.2	-163.8	-171.6	15.4
ΔE_{Pauli}	0.0	0.0	0.0	0.0
ΔE_{elstat}	-179.2	-148.1	-171.2	31.1
ΔE_{dist}	1.0	0.0	0.2	-1.0
Atomic charge on H:				
q_H (Hirshfeld)	0.13	0.14	0.18	-
q_H (Vornoi)	0.16	0.20	0.21	-

[a] $\Delta E_{total}=\Delta E_{orb}+\Delta E_{Pauli}+\Delta E_{elstat}+\Delta E_{dist}$

[b] See labeling explanation given in Fig. 1. Doublet ground states of H and CN were used in ETS analysis

[c] Charged fragments H^+ and CN^- were used in ETS analysis

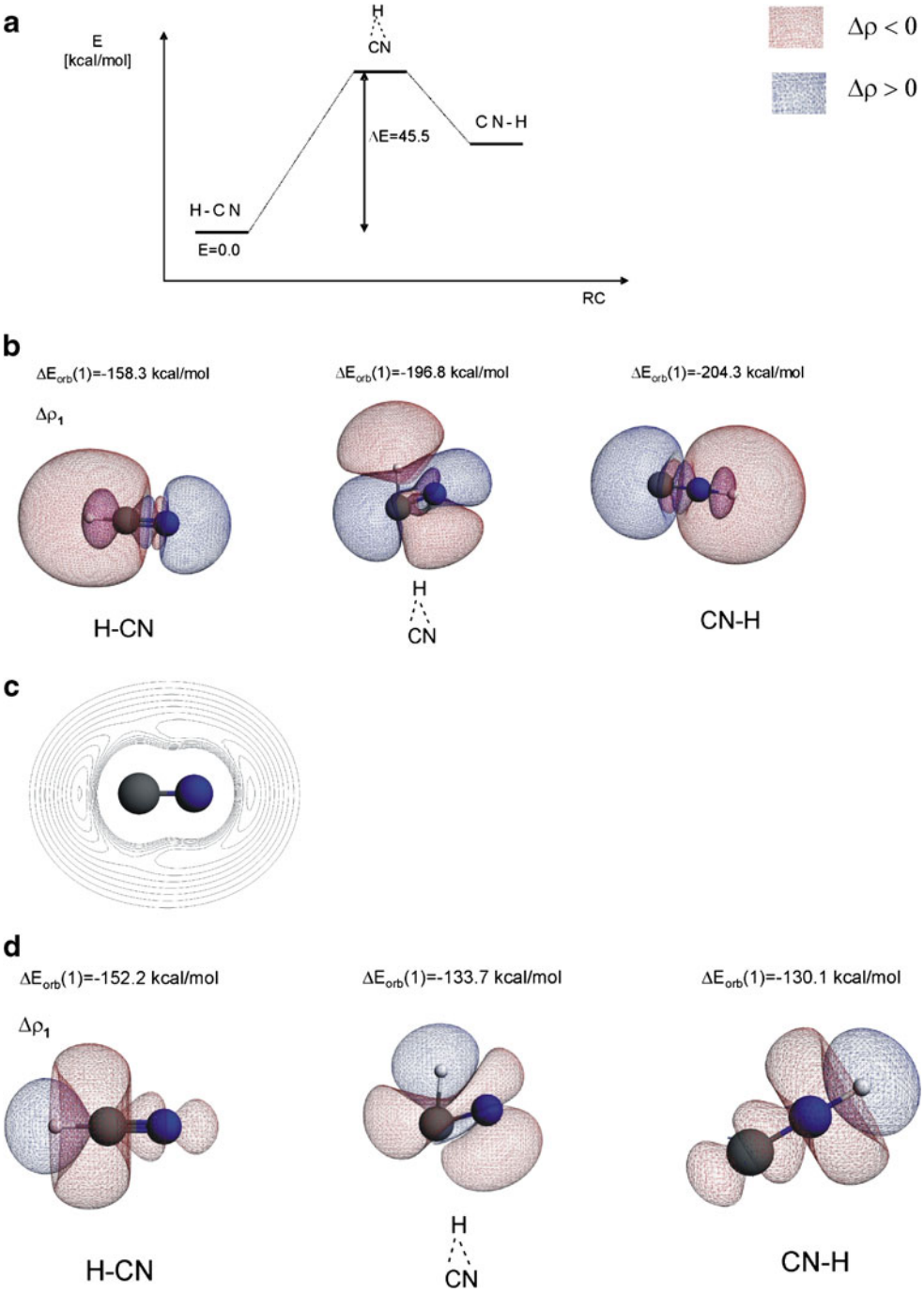

Fig. 2 **a** Energy profile of the isomerization HCN→CNH . Deformation density contributions, $\Delta\rho_1$, together with the corresponding energies for the substrate (**I-S**), transition state (**I-TS**) and product (**I-P**) are shown in **b** and **d** when applying the radicals (H· and CN·) and the charged fragments (H^+ and CN^-), respectively. **c** Molecular electrostatic potential (MEP) map for CN^-. The contour value is $|\Delta\rho|$=0.001 a.u. The *blue*/*red* contours correspond to accumulation/depletion of electron density

the geometry distortion term is negligible, as can be seen from Table 1. These results highlight the important role of Pauli destabilization, which is considered as the origin of steric repulsion [2, 22, 23, 27] in determination of the barrier to isomerization HCN→CNH when considering radical reference state, i.e., the bond between the radicals $H^{\cdot}$ and $CN^{\cdot}$.

As already discussed in the section on Theoretical background, a certain arbitrariness with the choice of the reference fragments exists when analyzing chemical reactions. Above, we presented results obtained with the radical fragment—this picture of the isomerization corresponds to the limiting case of hydrogen transfer from carbon towards nitrogen. However, yet another limiting case can be naturally considered for this reaction, corresponding to proton transfer. Thus, in the following, we present results of ETS-NOCV analysis for the HCN→CNH isomerization with the ionic reference state, i.e., considering H^+ and CN^- fragments.

This reference state is interesting for another reason. Because in the reference state all the electrons are located

on one (CN^-) fragment only, the Pauli repulsion contribution disappears by definition. Further, for each point of the reaction path, the electrostatic contribution, ΔE_{elstat}, is by definition equal to the molecular electrostatic potential (MEP) of the CN^- anion calculated in the respective proton position (since MEP corresponds to the interaction of the molecular species with the unitary point charge, i.e., proton). The contour map of the MEP calculated for CN^- is presented in Fig. 2c. For the anionic CN^- it is negative everywhere for larger distances from the nuclei, with two minima located in the vicinity of the carbon and nitrogen atoms. The minimum 'on the carbon side' is deeper than that 'on the nitrogen side'; this determines the electrostatic preference of the reactant (−179.2 kcal mol^{-1}, see the bottom part of Table 1 referring to ionic fragments) over the product (−171.2 kcal mol^{-1}). Further, it is obvious that the electrostatic contribution in the TS geometry must by less stabilizing (−148.1 kcal mol^{-1}). It is important to note that, with the radical reference state, as discussed earlier, the electrostatic term is more stabilizing for TS (−79.8 kcal mol^{-1}) than for the reactant (−48.7 kcal mol^{-1}), thus lowering the barrier by −31.1 kcal mol^{-1}, while with the ionic reference it is less stabilizing for TS, increasing the barrier by 31.1 kcal mol^{-1}. It must be emphasized that there is no contradiction between those two results, as they correspond to two, model, limiting cases corresponding to hydrogen-atom transfer, and proton transfer.

Let us now analyze the orbital interaction contributions, ΔE_{orb}, emerging with the ionic reference state, and the corresponding $\Delta\rho$ NOCV-contributions, presented in Fig. 2d. It can be expected that, for all the points along the reaction, with the ionic reference, a dominating $\Delta\rho_1$ contribution clearly shows the electron-transfer from CN^- towards the electron-less H^+. The corresponding orbital interaction energy contribution $\Delta E_{orb}(1)$ becomes less stabilizing along the reaction pathway: −152.2 kcal mol^{-1} for S, −133.7 kcal mol^{-1} for TS, and −130.1 kcal mol^{-1} for P. Thus, use of the ionic reference leads to the same conclusion as the radical reference, concerning the ionicity of hydrogen: here a decrease of $CN^- \rightarrow H^+$ electron transfer again corresponds to an increase in the charge on the hydrogen, as discussed above. Therefore, it may be concluded that, in the two limiting cases of radical and ionic reference fragments, one can obtain a complementary picture of the charge reorganization during the isomerization reaction, leading to consistent conclusions.

Reaction II: ethylene+butadiene cycloaddition

Let us now discuss the cycloaddition of ethene and 1,3-butadiene from the ETS-NOCV perspective (see reaction **II** in Fig. 1). At the initial stage of the reaction, we deal with isolated, non-interacting closed shell reagents, i.e., ethene and 1,3-butadiene. Consequently, each of the bonding contributions listed in Table 2 for **II-S** is equal to 0. As the two reactants approach each other during the reaction, the stabilizing interaction originating from orbital interaction term, ΔE_{orb}, emerges. The corresponding value in the transition state, **II-TS**, is ΔE_{orb} = −50.0 kcal mol^{-1}, see Table 2. It is necessary to remind ourselves that at **II-TS** we

Table 2 ETS[a] energy decomposition results (in kcal mol^{-1}) describing the bond between ethene and 1,3-butadiene for **II-S**, **II-TS**, **II-P**[b]. Singlet and triplet spin states were considered in ETS-NOCV analysis

ETS results	Ethene+1,3-butadiene II-S	TS II-TS	Cyclohexene II-P	$\Delta E^{\#}$ [(II-TS)-(II-S)]
Fragments in the singlet spin state				
ΔE_{total}[c]	0.0	12.8	-37.3	12.8
ΔE_{orb}	0.0	-50.0	-428.9	-50.0
ΔE_{Pauli}	0.0	92.9	501.2	92.9
ΔE_{elstat}	0.0	-50.0	-254.6	-50.0
ΔE_{dist}	0.0	19.8	145.0	19.8
Fragments in the triplet spin state				
ΔE_{total}[d]	0.0	12.8	-37.3	12.8
ΔE_{orb}	-83.6	-171.6	-404.3	-88.0
ΔE_{Pauli}	0.0	84.8	489.6	84.8
ΔE_{elstat}	0.0	-58.0	-297.7	-58.0
ΔE_{dist}	83.6	157.6	175.1	74.0

[a] $\Delta E_{total}=\Delta E_{orb}+\Delta E_{Pauli}+\Delta E_{elstat}+\Delta E_{dist}$

[b] See explanation given in Fig. 1

[c] Fragments in singlet state were considered in ETS analysis

[d] Fragments in triplet state were considered in ETS analysis. Distortion energy, ΔE_{dist}, calculated with respect to the singlet ground state of ethene and 1,3-butadiene

also used the singlet spin states for fragments (so-called reactants perspective approach). This is due to the "early" character of the TS, i.e., minor geometry changes are observed as compared to isolated ethene and 1,3 butadiene (see Scheme S1 in the electronic supplementary information).

It is evident from the contour of the dominant deformation density contribution, $\Delta\rho_1$, presented in Fig. 3b, that two C–C bonds between ethene and 1,3-butadiene molecules are formed in the transition state, **II-TS**. This is clearly represented by an outflow of electrons from the occupied π-orbital of ethene and accumulation of electron density in the bonding regions of C(ethene)–$C_{terminal}$(1,3-butadiene). It is also gratifying to see from the contour of $\Delta\rho_1$ that, in the TS, the new π-component of the C–C bond

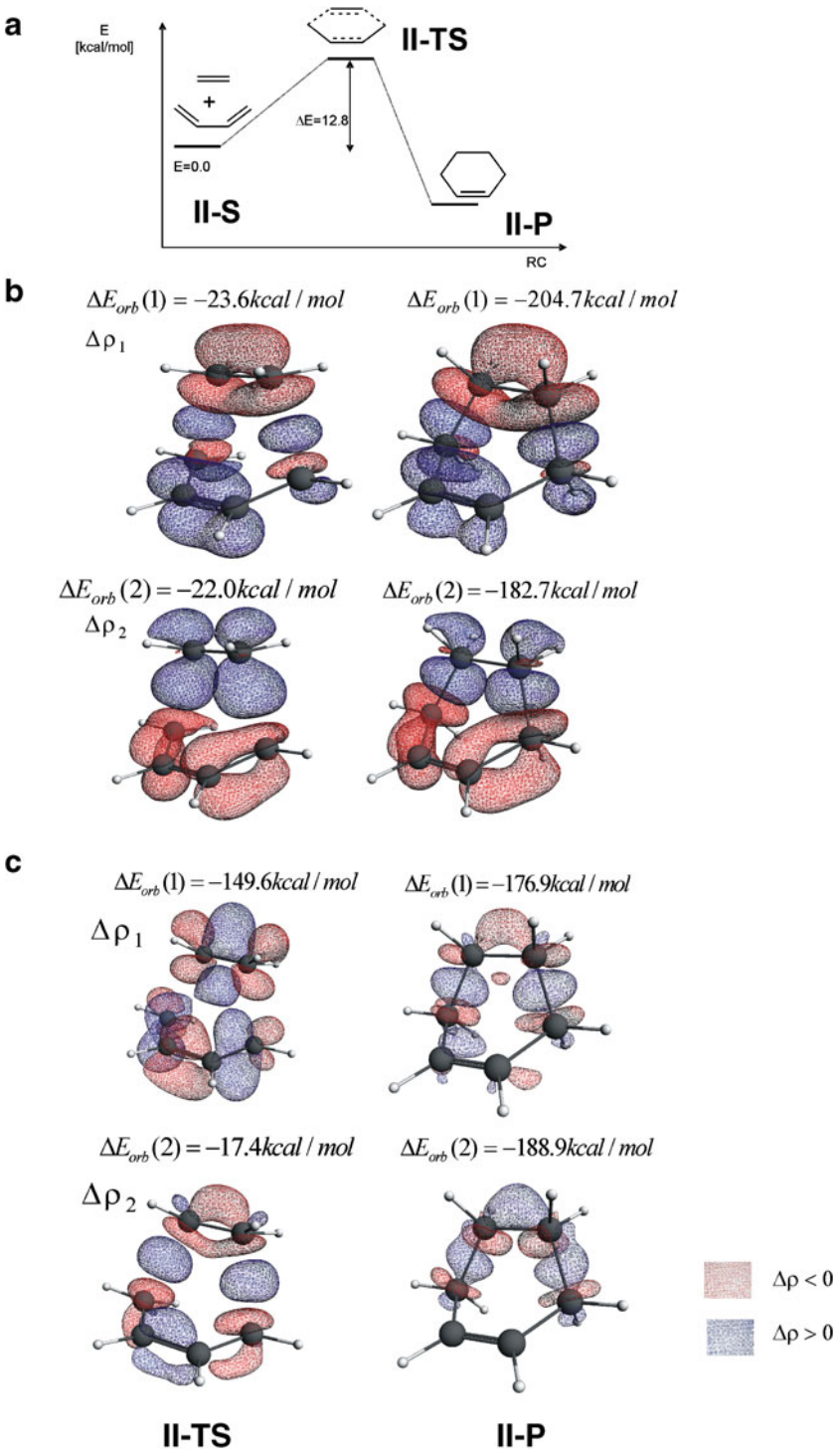

Fig. 3 Energy profile of the cycloaddition of ethene to 1,3-butadiene (panel **A**). Deformation density contributions, $\Delta\rho_1$ and $\Delta\rho_2$, together with the corresponding energies for the transition state (**II-TS**) and product (**II-P**) are shown in panel **B** (singlet reference state). The contour value is $|\Delta\rho|$ = 0.005 a.u. for **II-P** and 0.002a.u. for **II-TS**. In the case of the product triplet spin states for ethene (↑↑) and 1,3-butadiene (↓↓) were also considered (panel **C**)

is being formed, which indicates an early stage of formation of cyclohexene. These electron transfers lead to the stabilization of **II-TS**, $\Delta E_{orb}(1)=-23.6$ kcal mol^{-1}. The second quantitatively important [$\Delta E_{orb}(2) = -22.0$ kcal mol^{-1}] contribution comes from $\Delta\rho_2$, which exhibits depletion of electrons from the bonding π(C=C) orbitals of 1,3-butadiene and its accumulation into the bonding regions of C(ethene)–$C_{terminal}$(1,3-butadiene) and the anti-bonding π*(C=C) of ethene, see Fig. 3b.

It is necessary to point out that, apart from the orbital interaction term, additional stabilization of **II-TS**, of the same magnitude, i.e., −50.0 kcal mol^{-1}, comes from the electrostatic contribution (ΔE_{elstat}), see Table 2. However, an inclusion of the destabilizing factors, i.e., the Pauli repulsion and distortion energy terms, leads to overbalance of the stabilization and, accordingly, the activation barrier of the addition emerges and is given by $\Delta E^{\#} = \Delta E_{total}$(**I-TS**)$-\Delta E_{total}$(**I-S**)$=12.8$ kcal mol^{-1}. DFT calculations by Osuna and Houk [40] based on different computational details provide a higher $\Delta E^{\#} = 18.5$ kcal mol^{-1}. It is interesting to note that, when considering solely destabilization of **II-TS** originating from the Pauli repulsion contribution, the cycloaddition would proceed without activation barrier—an exclusion of the changes in ΔE_{dist} along the reaction path would give negative $\Delta E^{\#} = -7.1$ kcal mol^{-1}, see Table 2. This shows that, in the case of this reaction, a significant degree of structural deformation of the reactants measured by the geometry distortion energy plays an important role in determination of the barrier to cycloaddition. Osuna and Houk [40] also calculated the distortion energy (at B3LYP level of theory) and their value of 23.6 kcal mol^{-1} compares well with our ΔE_{dist}=19.8 kcal mol^{-1}.

Finally, for comparison, we also performed ETS-NOCV analysis of the reaction path from the product perspective, i.e., the triplet spin states for ethene and 1,3-butadiene were used for both cyclohexene (**II-P**) and the transition state **II-TS**. The results were added as new entries in Table 2 and Fig. 3c.

It can be seen in the case of cyclohexene constituted from the triplet fragments that the orbital interaction term dominates in the stabilization as compared to electrostatic factor (the same is true when applying the singlet spin states for fragments). Deformation density contributions, presented in Fig. 3c, for **II-P** clearly show the formation of strong covalent C–C bonds [$\Delta E_{orb}(1)=-176.9$ kcal mol^{-1} and $\Delta E_{orb}(2)=-188.9$ kcal mol^{-1}].

However, it should be emphasized for **II-P** that, in the picture resulting from the reactants perspective (closed-shell fragments), an overall bonding picture resulting from a sum of the ‘donation’ and ‘back-bonding’ contributions shown in Fig. 3b will be qualitatively similar to that obtained from a summation of the ‘covalent’ contributions (product perspective, from the triplet fragments) shown in Fig. 3c. The orbital energy part originating from the two major components in the triplet-reference-state, $\Delta E_{orb}(1)+\Delta E_{orb}(2)=$ (−176.9 kcal mol^{-1}) + (−188.9 kcal mol^{-1}) = −365.8 kcal mol^{-1} is smaller than the orbital energy part originating from the two major components in the singlet-reference-state, $\Delta E_{orb}(1)+\Delta E_{orb}(2)$ = (−204.7 kcal mol^{-1})+(−182.7 kcal mol^{-1}) = −387.4 kcal mol^{-1}. This indicates that the bond description is more compact in the case of the singlet-reference-state since, in the case of the triplet-reference state, the larger part of the charge-flow must be hidden in many of the small-energy components (corresponding to small NOCV eigenvalues).

Let us now discuss the electronic structure of the TS that is built from ethene and butadiene in the triplet spin state (i.e., the product perspective). It can be seen from Fig. 3c that dominant contribution [$\Delta E_{orb}(1)=-149.6$ kcal mol^{-1}] to the deformation density originates from the polarization of the reactants, which clearly leads to the strengthening of the C–C bond in ethene and the terminal C–C bonds (‘double’ C–C bonds) of butadiene. Thus, this contribution corresponds to the ‘relaxation’ of the π-electron density from a triplet towards the singlet state of reactants. This, in our opinion, shows that a singlet reference state is more appropriate for a description of the TS for this reaction. This could be intuitively expected from the early-TS character of the TS discussed.

The second NOCV contribution, which corresponds to much smaller orbital-interaction energy, $\Delta E_{orb}(2)=-17.4$ kcal mol^{-1}, exhibits electron density changes towards the product, i.e., formation of covalent C–C bonds between the fragments, and strengthening of the middle C–C butadiene bond (becoming a ‘double’ bond in the product), at the expense of ‘terminal’ C–C bonds of butadiene (becoming ‘single’ bonds in the product).

Finally, one should note that the Pauli repulsion component is slightly smaller for the triplet-reference state than in the case of singlet fragments (84.8 kcal mol^{-1} vs 92.9 kcal mol^{-1}), but is still important for TS destabilization. Thus, both obtained pictures of bonding (with singlet and triplet states for the considered fragments), highlight the importance of Pauli repulsion and geometry reorganization in the destabilization of the TS.

Reaction III

One of the crucial steps in the olefin polymerization cycle catalyzed by organometallic complexes is the migratory insertion of the olefinic monomer into the metal-alkyl bond via a TS in which the metal ion, the α-carbon atom of the alkyl, and the two carbon atoms of the monomer participate in the bond formation / bond breaking process. As a result, a new carbon–carbon bond is formed and a polymer chain is elongated by a two-carbon unit. As presented in Fig. 1 (reaction **III**), the backside (BS) propagation mechanism

starts from the π-complex, in which an incoming olefin (ethylene) is coordinated to the electron-deficient metal center of the β-agostic alkyl complex in the position anti (i.e., BS) to the β-agostic bond (labeled as **III-S** in the figure). Proceeding via a four-centered TS stabilized by a strong β-agostic interaction (**III-TS**), the insertion of the monomer leads to a δ-agostic alkyl complex as a direct product of the reaction (**III-P**). As stated in the Computational details section for **III-S** and **III-TS**, we used primarily the singlet spin state for ethene and Ti-containing catalyst (reactant perspective). For completeness, we also present the full ETS-NOCV results when applying triplet spin states for fragments in the electronic supplementary information (Table S2 and Fig. S1).

We will start the discussion with a description of the BS insertion reaction on the basis of deformation density contributions originating from NOCVs, $\Delta\rho_k$, and the corresponding energies, ΔE_{orb} (k). The two dominating components of the deformation density, $\Delta\rho_1$ and $\Delta\rho_2$, describing the bond between ethylene molecule and the remaining Ti-based fragment for both the BS π-complex and TS together with the corresponding energy values are presented in Fig. 4.

Let us first discuss the main NOCV deformation density component, $\Delta\rho_1$, in **III-S** geometry. As can be seen, this demonstrates the accumulation of electron density in the region between the outer ethylene carbon atom and the titanium center corresponding to the Ti–ethylene bond formation, as well as the depletion of electron density from the double C=C ethylene as well as Ti–α-C(propyl) bonds. The corresponding deformation density contribution in the **III-TS** structure reveals a significant similarity to the contour described above. As in the case of **III-S**, it presents not only the Ti–C(ethylene) bond, but primarily further electron density rearrangements in the monomer-polymer region initiated already at the π-complex stage. According to the direction of the charge flow, such rearrangements can be identified with the following processes: (1) transformation of the double C=C bond in the ethylene molecule into the single C–C; (2) rupture of the Ti–α-C(propyl) bond; and, finally (3) formation of the new covalent C(ethylene)–α-C(propyl) bond. When going from the reagent to the TS, an increased orbital interaction between ethylene and the Ti-based fragment is noted, $\Delta E_{orb}(1)$, by −21.9 and −64.6 kcal mol^{-1}. This might be linked to the strengthening of the Ti–C(ethylene) bond and formation of a strong covalent C–C connection. As far

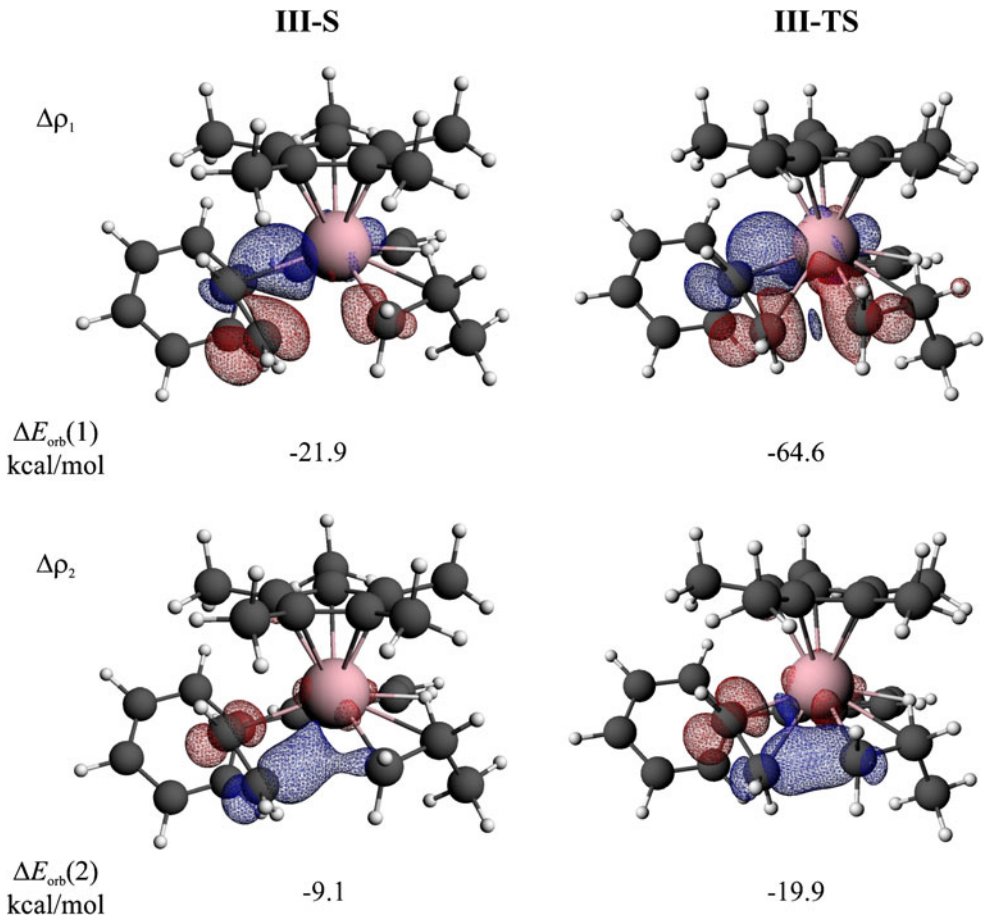

Fig. 4 Dominating contributions to the deformation density $\Delta\rho$ describing the bond between ethylene and titanium-based fragments for the **III-S** and **III-TS** structures according to ETS-NOCV analysis. The contour value is $|\Delta\rho|$=0.003 a.u. The *blue*/*red* contours corresponds to accumulation/depletion of electron density

as the second NOCV-based deformation density contribution, $\Delta\rho_2$, is concerned, one can see that, in **III-S**, it presents a delocalized bonding between the inner ethylene carbon atom and both the metal center and the alkyl group. In the TS, such bonding becomes localized predominately in the region of inner C(ethylene)–α-C(propyl). The corresponding stabilization $\Delta E_{orb}(2)$ is −9.1 and −19.9 kcal mol^{-1} for **III-S** and **III-TS**, respectively. It is clearly seen that these are definitely of less importance compared to the former pair of the deformation density contributions, $\Delta E_{orb}(1)$ = −21.9 and −64.6 kcal mol^{-1}. An increase in $\Delta E_{orb}(1)$ and $\Delta E_{orb}(2)$ values determines the trend of increasing stabilization in the total ΔE_{orb} values, −39.5 kcal mol^{-1} for **III-S** and −100.2 kcal mol^{-1} for **III-TS**, ΔE_{orb}**(III-TS)**−ΔE_{orb}**(III-S)**= −60.7 kcal mol^{-1}, see Table 3.

The results collected in Table 3 show that the increase in stabilization originating from total orbital interaction and the electrostatic terms when going from **III**-S to **III**-TS is overcompensated by the two destabilizing factors, i.e., Pauli repulsion and geometry distortion contributions. As a final result, the reaction considered reveals the low activation barrier of ΔE_{total}**(III-TS)**−ΔE_{total}**(III-S)**=2.2 kcal mol^{-1}. It is also clearly seen from Table 3 that the Pauli repulsion term is predominately responsible for the existence of the activation barrier.

As we go from **III-TS** to the product **III-P**, a drop in total bonding energy is observed (from −4.9 kcal mol^{-1} to −19.1 kcal mol^{-1}). The 'product' columns of Table 3 show that the drop in ΔE_{total} values is due to a decrease in both orbital and electrostatic contributions, with the notable dominance of the former. In addition, the Pauli respulsion term is more important in the destabilization as compared to the distortion energy contribution. This conclusion is consistent when considering both triplet and singlet spin states for ethene and Ti-containing catalyst (see Table 3). The results concerning a description of the TS and substrate from the 'product' perspective are shown in the Supporting Information (Table S3). Similarly, to the cycloaddition reaction, the singlet-reference fragments are more appropriate for a description of the TS for ethylene insertion discussed here, due to its early-TS-character.

Reaction IV

As a final example, we will study selective activation of the B–H bond catalyzed by an Ir-catalyst (see reaction **IV** in Fig. 1). Our investigation is prompted by the experimental work of Rossin and coworkers [46], in which these authors have shown that solely the B–H bond of ammonia borane (AB) is activated. In this latter work, the authors also noticed that, surprisingly "…Very little attention has so far been devoted to the understanding of whether B–H versus N–H activation is preferred….". Therefore, in this section we will characterize not only the energy profile based on the ETS-NOCV method but also rationalize the origin of B–H bond activation.

In the first step, we analyzed possible bonding modes of AB to the Ir-catalyst. As a result we found two stable complexes of AB with the metal-catalyst (see structures **IV-S** and **IV-S'** in Fig. 5). In the former case, AB interacts with the Ir-center via the B–H bond whereas, in the latter, AB forms the bonding with Ir-catalyst via the NH_3 group. Keeping in mind that experimental data show that solely the B–H bond of AB is activated, it is thus not surprising that the conformer **IV-S** is more stable (by 4.4 kcal mol^{-1}) than the structure **IV-S'**. The ETS results describing the interaction of AB with the Ir-catalyst presented in Fig. 5 show that this is due to the higher stabilization originating from electrostatic (ΔE_{elstat} is lower by 44.8 kcal mol^{-1}) and orbital interaction (ΔE_{orb} is lower by 17.6 kcal mol^{-1}) contributions. An important question that arises at this point is why AB prefers an orientation that is suitable for activation of the B–H bond. The Hirshfeld's atomic charges calculated for free AB show that the BH_3 group is more negatively charged than the NH_3 unit (see Fig. 6a). Accordingly, the negative MEP occurs in the vicinity of

Table 3 ETS[a] energy decomposition results (in kcal mol^{-1}) describing the bond between ethylene and Ti-based fragment for **III-S** and **III-TS**[b]

ETS results	π-complex III-S	TS III-TS	δ-agostic product III-P	$\Delta E^{\#}$ [(III-TS)-(III-S)]	δ-agostic product III-P[d]
ΔE_{total}[c]	-7.1	-4.9	-19.1	2.2	-19.1
ΔE_{orb}	-39.5	-100.2	-494.8	-60.7	-306.9
ΔE_{Pauli}	69.1	165.4	592.4	96.3	387.0
ΔE_{elstat}	-50.9	-101.1	-280.8	-50.2	-246.6
ΔE_{dist}	14.2	31.0	164.1	16.8	147.4

[a] $\Delta E_{total}=\Delta E_{orb}+\Delta E_{Pauli}+\Delta E_{elstat}+\Delta E_{dist}$

[b] See explanation in Fig. 1

[c] Fragments in singlet state were considered

[d] Fragments in triplet state were considered. Distortion energy, ΔE_{dist}, calculated with respect to the singlet ground state of ethene and Ti-containing catalyst

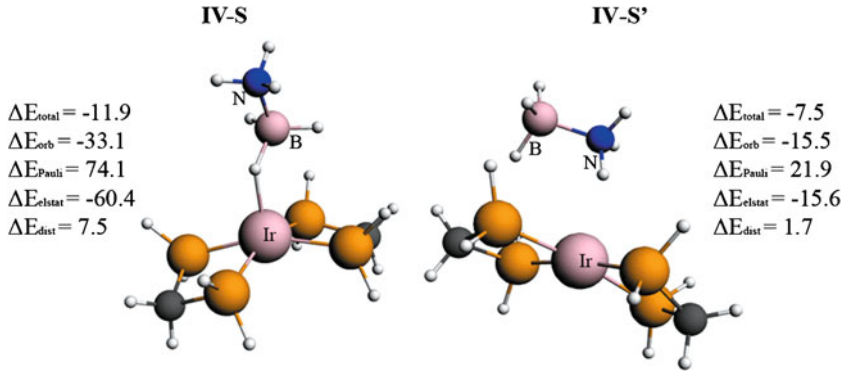

Fig. 5 Stable complexes of ammonia borane (AB) with Ir-containing catalyst. **IV-S** labels the structure where B–H bond is elongated, whereas **IV-S'** shows the binding of AB to the catalyst via the NH_3 group. ETS results (in kcal mol^{-1}) of the interaction between AB and the catalyst are also presented

BH_3 unit, as can be seen from Fig. 6b. Therefore, AB tends to attack the electrophilic Ir center (with positive MEP potential) via solely the BH_3 group. It can be seen clearly that the electrostatic factor not only explains the origin of binding of AB with the Ir-center via the BH_3 group, but it also introduces very high stabilization to the already formed complex, **IV-S** (see ETS results presented in Fig. 5).

Let us now switch our attention to analysis of the changes in electronic structure during the reaction of B–H bond activation. Figure 7b presents the leading contours of deformation density contributions based on NOCVs with the corresponding energies. The main contribution to ΔE_{orb} comes from the charge rearrangement, $\Delta\rho_1$. In **IV-S**, $\Delta\rho_1$ captures the formation of the B–H bond and the newly formed Ir–H connection, which corresponds to stabilization by $\Delta E_{orb}(1)= -103.5$ kcal mol^{-1}. In the TS, **IV-TS**, one can see not only the Ir–H bond formed (and the practically broken B–H bond) but also the new Ir–B interaction, which is reflected in further stabilization $\Delta E_{orb}(1)= -125.3$ kcal mol^{-1}. The second deformation density contribution, $\Delta\rho_2$, participating in ΔE_{orb} represents a dative component, i.e., an outflow of electrons from the Ir center to hydrogen, see $\Delta\rho_2$ (the same qualitative picture for **IV-S** and **IV-TS**). It becomes constantly more stabilizing when going from (**IV-S**) to (**IV-TS**), $\Delta E_{orb}(2)$ varies from −9.1 kcal mol^{-1}, up to −13.7 kcal mol^{-1}. It is worth noting that the charge flow estimations, $\Delta q(k)$, obtained from NOCV eigenvalues (see the Table S1 of in the electronic supplementary material) exhibit the same trend as energetic flow measures, $\Delta E_{orb}(k)$. In addition, we found that boron and iridium atoms lose electrons according to Voronoi charge analysis when going from **IV-S** to **IV-TS**, Δq(**S→TS**, Ir)=+0.10e, Δq(**S→TS**, B)=+0.17e. This is in qualitative line with the charge and electronic estimations of the density transfer $\Delta\rho_1$ (where charge depletion from boron and iridium atoms was similarly noted).

It is crucial to point out that the electronic factor, ΔE_{orb}(**IV-TS**)-ΔE_{orb}(**IV-S**)= −41.1 kcal mol^{-1}, is quantitatively less important in the stabilization of the TS as compared to the stabilization that originates from the electrostatic contribution, ΔE_{elstat}(**IV-TS**)-ΔE_{elstat}(**IV-S**)= −95.7 kcal mol^{-1}. Similarly to the previous reactions studied, the Pauli repulsion (by 122.3 kcal mol^{-1}) is mostly responsible for the emerging of the activation barrier, $\Delta E^{\#}=\Delta E_{total}$(**IV-TS**)−$\Delta E_{total}$(**IV-S**)= 3.8 kcal mol^{-1}. Rossin et al. [46] obtained $\Delta E^{\#}$=4.3 kcal mol^{-1}.

It should also be noted that, alternatively, we used the two closed shell fragments (NH_3BH_3 and Ir-catalyst) in the singlet spin state in order to analyze the changes in electronic structure when going from **IV-S** to **IV-TS**. The ETS results presented in Table 4 show a consistent trend as compared to the three fragment-based approach. Namely, the electrostatic stabilization dominates over the orbital interaction factor in the stabilization of **IV-TS**. On the other hand, steric hindrance due to the Pauli repulsion term is the most important in the destabilization of **IV-TS**.

It is worth noting that, when we go from transition state **IV-TS** to product **IV-P** , further stabilization stemming from electrostatic and orbital interaction term is observed (see Table 5), by ΔE_{elstat}(**IV-P**)-ΔE_{elstat}(**IV-TS**)= −61.5 and ΔE_{orb}(**IV-P**)−ΔE_{orb}(**IV-TS**)= −74.1 kcal mol^{-1}, respectively.

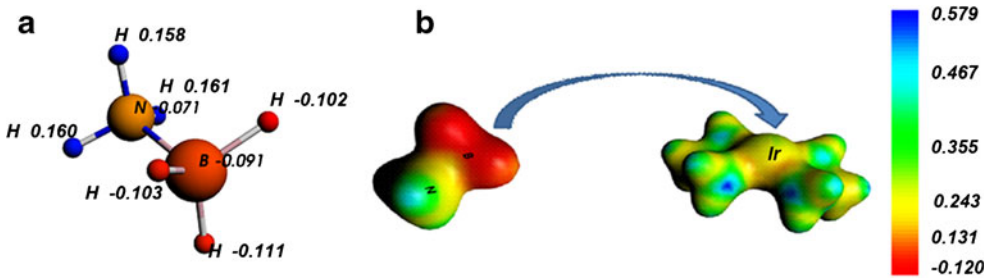

Fig. 6 **a** Hirshfeld's atomic charges on the AB molecule, **b** MEP map around AB and the Ir-catalyst

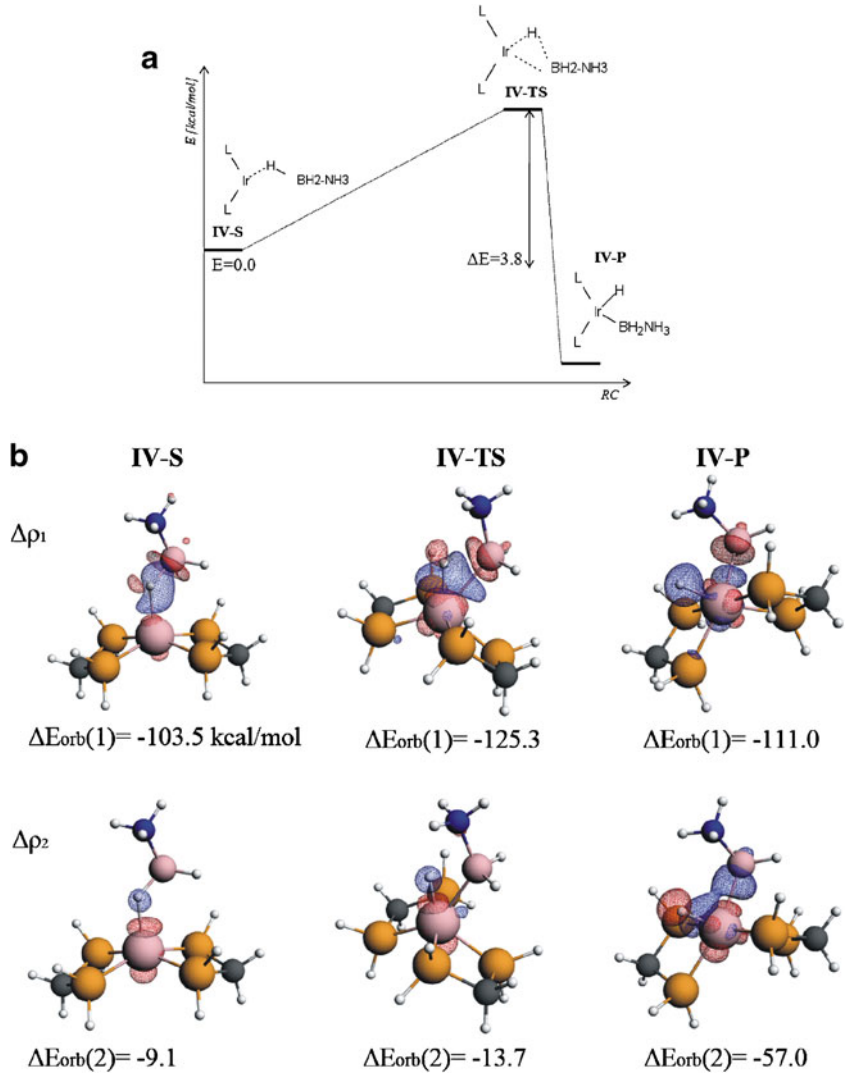

Fig. 7 Energy profile of B–H bond activation catalyzed by an Ir-based complex. **b** Contours of deformation density contributions $\Delta\rho_1$, $\Delta\rho_2$ and the corresponding energies for **IV-S**, **IV-TS** and **IV-P**. *Red areas* of $\Delta\rho_i$ shows charge depletion, whereas *blue areas* indicate charge accumulation upon bond formation. The contour value is $|\Delta\rho|$=0.001 a.u

This leads to overcompensation of the destabilization originating from the distortion and Pauli repulsion terms and accordingly results in the exothermicity of the reaction ΔE_{total}**(IV-P)**$-\Delta E_{\text{total}}$**(IV-S)**= −12.8 kcal mol^{-1}. It should be noted that, when applying not singlet, but triplet spin state for the Ir-containing fragment in the case of the product **IV-P**, the electrostatic term changes similarly: ΔE_{elstat}**(IV-P)**$-\Delta E_{\text{elstat}}$**(IV-TS)**= −63.8 kcal mol^{-1}, although the orbital interaction contribution is notably less stabilizing ΔE_{orb}**(IV-P)**$-\Delta E_{\text{orb}}$**(IV-TS)**= −26.0 kcal mol^{-1}. Both pictures, however, consistently show the dominance of the electrostatic stabilization in the product **IV-P**.

Table 4 ETS[a] energy decomposition results (in kcal mol^{-1}) describing the interaction between two closed shell fragments NH_3BH_3 and Ir-catalyst for **IV-S** and **IV-TS**

ETS results	IV-S	IV-TS	$\Delta E^{\#}$ [(IV-TS)-(IV-S)][b]
ΔE_{total}	-12.0	-8.2	3.8
ΔE_{orb}	-33.2	-86.3	-53.1
ΔE_{Pauli}	74.1	208.6	134.5
ΔE_{elstat}	-60.5	-174.4	-113.9
ΔE_{dist}	7.5	43.8	36.3

[a] $\Delta E_{\text{total}}=\Delta E_{\text{orb}}+\Delta E_{\text{Pauli}}+\Delta E_{\text{elstat}}+\Delta E_{\text{dist}}$

[b] See labeling in Fig. 1

Finally, we performed ETS-NOCV analysis of **IV-S**, **IV-TS** and **IV-P** when applying charged fragments in the singlet states: H^+, $NH_3BH_2^-$ and Ir-containing catalyst. The results are presented in Table S3 of the electronic supplementary information file. Although, we do not present a detailed analysis in the body of the manuscript, it is important to note that decomposition of $\Delta E^{\#}$ into the specific bonding contributions leads to similar conclusions as compared to those obtained from three fragments-based approach (H↑, ↓BH_2NH_3 and closed shell Ir-catalyst). Namely, the low barrier of activation of B–H bond originates predominantly from the large electrostatic stabilization of **IV-TS**. On the

Table 5 ETS[a] energy decomposition results (in kcal mol^{-1}) describing the interaction between three sub-systems (H↑, NH_3H_2B↓ and closed shell Ir-catalyst) for **IV-S**, **IV-TS**, **IV-P**[b]

ETS results	IV-S	IV-TS	IV-P[c]	$\Delta E^{\#}$ [(IV-TS)-(IV-S)]	IV-P[d]
ΔE_{total}	-119.8	-116.0	-132.6	3.8	-132.6
ΔE_{orb}	-121.4	-162.5	-236.6	-41.1	-188.5
ΔE_{Pauli}	135.5	257.8	363.2	122.3	313.6
ΔE_{elstat}	-141.6	-235.3	-296.8	-95.7	-299.1
ΔE_{dist}	7.7	24.0	37.6	16.3	41.4

[a] $\Delta E_{total}=\Delta E_{orb}+\Delta E_{Pauli}+\Delta E_{elstat}+\Delta E_{dist}$

[b] See explanation given in Fig. 1

[c] The following fragments, H↑, NH_3H_2B↓ and singlet Ir-catalyst, were considered

[d] The following fragments, H↑, NH_3H_2B↓ and triplet Ir-catalyst (↑↑), were considered, distortion given with respect to doublet H and NH_3BH_2 fragments and singlet Ir-based catalyst

other hand, a positive value of $\Delta E^{\#}$ originates predominantly from the Pauli repulsion contribution.

Due to the fact that the electrostatic term appears to be the crucial stabilizing factor of the TS (independently of the type of reference states used in ETS-NOCV analysis) one can envisage that use of strongly electrophilic metal centers should provide a very effective way of dehydrogenation of AB that proceeds via a mechanism based on B–H bond activation. Indeed, very recently, the palladium cationic system containing acetonitrile ligands was used for dehydrogenation of AB via B–H bond activation, and proved to exhibit the best performance to date [60].

Finally, it should be noted that Bickelhaupt and Zeist recently used a pure ETS-scheme in their so-called "activation strain model", which allowed, for example, an understanding of the activation barriers of C–H bond activation or nucleophilic substitution S_N2 [27]. In addition, Fernàndez et al. recently applied the activation strain model to double group transfer reactions [61]. In our present study, however, we not only used the original ETS scheme to analyze the origin of activation barriers for reactions of significant catalytic importance but, primarily, we applied an NOCV-originated study based on charge flow channels that allowed us to understand density reorganization both qualitatively and quantitatively during the course of the considered reactions.

Concluding remarks

In the present account, we have analyzed the changes in electronic structure during chemical reactions based on the combined charge and energy decomposition scheme ETS-NOCV. In addition, decomposition of the activation barrier, $\Delta E^{\#}$, into stabilizing (electronic and electrostatic) and destabilizing (Pauli repulsion and distortion energy) factors was discussed. As examples, we chose two simple model reactions, namely (**I**) hydrogen cyanide to hydrogen isocyanide, HCN→CNH isomerization; and (**II**) Diels-Alder cycloaddition of ethene to 1,3-butadiene; and two more complex examples of catalytic reactions, i.e., (**III**) BS insertion of ethylene into the metal-alkyl bond in half-titanocene with phenyl-phenoxy ligand catalyst; and (**IV**) B–H bond activation catalyzed by an Ir-containing catalyst. Various reference states were considered in the bonding analysis for each of the reactions under study.

We found that NOCV-based deformation densities ($\Delta\rho_i$) and the corresponding energies [ΔE_{orb}(i)] provided a very useful, qualitative and quantitative, picture of the chemical bonds breaking and forming during the course of the reaction. Consequently, this yields a compact characterization of electronic charge reorganization along the considered pathways (**I**, **II**, **III** and **IV**). In addition, ETS-NOCV allowed the activation barrier to be characterized in terms of stabilizing and destabilizing factors.

We found that reactions (**I**) and (**II**) exhibited the highest barriers of activation, at $\Delta E^{\#}$=45.5 kcal mol^{-1} and $\Delta E^{\#}$= 12.8 kcal mol^{-1}, respectively. Decomposition of the barrier into stabilizing (electronic and electrostatic) and destabilizing (Pauli repulsion and geometry distortion) contributions led to the conclusion that the main factor responsible for such high values of $\Delta E^{\#}$ for **I** and **II** is the Pauli repulsion contribution, which is the origin of steric interaction [2]. In addition, in the case of cycloaddition of ethene to 1,3-butadiene, a significant degree of structural deformation of the reactants, as measured by the geometry distortion energy, ΔE_{dist}, plays an important destabilizing role. In both reactions, stabilization of the TSs (relatively to the reactants) originating from both electronic (ΔE_{orb}) and electrostatic (ΔE_{elstat}) contributions appeared to be very important, with the evident dominance of ΔE_{orb} (over ΔE_{elstat}) in the case of **I**. The above conclusions are valid for reaction **II** when applying both singlet and triplet reference states.

Catalytic reactions (**III**) and (**IV**) proceed relatively easily; the calculated barriers are 2.2 and 3.8 kcal mol^{-1},

respectively. The main factors responsible for high stabilization of the TS of these processes, **III-TS** and **IV-TS**, are the electronic term (ΔE_{orb}) in the case of reaction **III** and the electrostatic attraction (ΔE_{elstat}) for B–H bond activation in reaction **IV**. The remaining stabilizing components, i.e., ΔE_{elstat} for **III** and ΔE_{orb} for **IV** are quantitatively less important. In both cases, destabilization originating from Pauli repulsion is crucial in overcompensation of the total stabilization (stemming from the electronic and electrostatic contributions). In the case of reaction **IV**, we found that the electrostatic term is not only predominantly responsible for the low activation barrier of the B–H bond, but it also causes suitable orientation of AB with respect to the catalyst, i.e., AB attacks the electrophilic Ir-center via the negatively charged BH_3 unit. It should be noted that, ver recently, strongly electrophilic Pd(II)-containing catalysts have been used in the catalytic dehydrogenation of AB that proceeds via B–H bond activation. This reaction appears to exhibit the best performance to date [60]. This is in agreement with our finding that catalysts containing strong Lewis acid-type metal centers should be appropriate candidates for effective dehydrogenation of AB that proceeds via a mechanism based on B–H bond activation. Further studies on the dehydrogenation of AB by other catalysts containing cationic metal centers are ongoing. These results show that application of the ETS-NOCV method has opened up new directions for the development of effective and cheap catalysts for dehydrogenation of AB. The above conclusions on factors determining the barrier to activation of the B–H bond are true when considering different reference states.

Finally, it is important to emphasize that use of the ETS-NOCV method for analysis of the catalytic reaction allows for extraction of the information on the role of the catalyst. Namely, in the case of B–H bond breaking of AB, we found that the Ir-based catalyst significantly lowers the barrier by up to 3.8 kcal mol^{-1}, as compared to non-catalytic rupture of B–H bond, by 102.1 kcal mol^{-1} (the calculations by Rablen and Hartwig at the level of G-2 theory) [62]. As stated previously, such lowering stems predominantly from the electrostatic interaction between negatively charged BH_3 of AB and the electrophilic Ir-center; electronic stabilization originating from the orbital interaction term between AB and the metal center is less important. This is opposite to the case, for example, of the insertion reaction of ethene (labeled **III** in Fig. 1), where the electronic term appears to be dominant over the electrostatic factor in stabilization of the TS.

Acknowledgments M.P.M. greatly acknowledges the financial support of the Foundation for Polish Science ("START" scholarship) as well as from the Polish Ministry of Science and Higher Education ("Outstanding Young Researchers" scholarship).

References

1. Frenking G, Frohlich N (2000) Chem Rev 100:717–774, and references therein
2. Bickelhaupt FM, Baerends EJ (2000) Kohn-Sham density functional theory: predicting and understanding chemistry. In: Lipkowitz KB, Boyd DB (eds) Reviews in computational chemistry, vol 15. Wiley, New York, pp 1–86
3. Hund F (1926) Z Phys 36:657–674
4. Mulliken RS (1927) Phys Rev 29:637–649
5. Boys SF (1960) Mol Phys 32:296–299
6. Edmiston C, Ruedenberg K (1963) Rev Mod Phys 35:457–464
7. Reed AE, Curtiss LA, Weinhold F (1998) Chem Rev 88:899–926
8. Wiberg K (1968) Tetrahedron 24:1083–1096
9. Gopinathan MS, Jug K (1983) Theor Chim Acta 63:497–509
10. Mayer I (1984) Chem Phys Lett 97:270–274
11. Nalewajski RF, Mrozek J (1994) Int J Quantum Chem 51:187–200
12. Nalewajski RF, Mrozek J, Formosinho SJ, Varandas AJC (1994) Int J Quantum Chem 52:1153–1176
13. Nalewajski RF, Mrozek J (1996) Int J Quantum Chem 57:377–389
14. Nalewajski RF, Mrozek J, Mazur G (1996) Can J Chem 74:1121–1130
15. Nalewajski RF, Mrozek J, Michalak A (1997) Int J Quantum Chem 61:589–601
16. Nalewajski RF, Mrozek J, Michalak A (1998) Pol J Chem 72:1779–1791
17. Michalak A, De Kock R, Ziegler T (2008) J Phys Chem A 112:7256–7263
18. Bader RF (1990) Atoms in molecules. A quantum theory. University Press, Oxford
19. Ponec R (1997) J Math Chem 21:323–333
20. Dapprich S, Frenking G (1995) J Phys Chem 99:9352–9362
21. Kitaura K, Morokuma K (1976) Int J Quantum Chem 10:325–340
22. Ziegler T, Rauk A (1977) Theor Chim Acta 46:1–10
23. Ziegler T, Rauk A (1979) Inorg Chem 18:1755–1759
24. Pendás AM, Blanco MA, Francisco E (2006) J Chem Phys 125:184112–184120
25. Jeziorski B, Moszynski R, Szalewicz K (1994) Chem Rev 94:1887–1930
26. Toro-Labbé A, Gutiérrez-Oliva S, Murray JS, Politzer P (2009) J Mol Model 15:707–710
27. Van Zeist WJ, Bickelhaupt FM (2010) Org Biomol Chem 8:3118–3127
28. Mitoraj M, Michalak A, Ziegler T (2009) J Chem Theor Comput 5:962–975
29. Mitoraj M, Michalak A, Ziegler T (2009) Organometallics 28:3727–3733
30. Broclawik E, Załucka J, Kozyra P, Mitoraj M, Datka J (2010) J Phys Chem C 114:9808–9816
31. Rejmak P, Mitoraj M, Broclawik E (2010) Phys Chem Chem Phys 12:2321–2330
32. Kurczab R, Mitoraj MP, Michalak A, Ziegler T (2010) J Phys Chem A 114:8581–8590
33. Mitoraj M, Michalak A (2007) J Mol Model 13:347–355
34. Mitoraj M, Michalak A (2007) Organometallics 26:6576–6580
35. Mitoraj M, Michalak A (2008) J Mol Model 14:681–687
36. Michalak A, Mitoraj M, Ziegler T (2008) J Phys Chem A 112:1933–1939
37. Mitoraj M, Zhu H, Michalak A, Ziegler T (2008) Int J Quantum Chem 109:3379–3386
38. Srebro M, Mitoraj M (2009) Organometallics 28:3650–3655
39. Michalak A, Ziegler T (2001) J Phys Chem A 105:4333–4343
40. Osuna S, Houk KN (2009) Chem Eur J 15:13219–13231
41. Margl P, Deng L, Ziegler T (1998) Organometallics 17:933–946
42. Margl P, Deng L, Ziegler T (1998) J Am Chem Soc 120:5517–5525

43. Kim TJ, Kim SK, Kim BJ, Hahn JS, Ok MA, Song JH, Shin DH, Ko J, Cheong M, Kim J, Won H, Mitoraj M, Srebro M, Michalak A, Kang SO (2009) Macromolecules 42:6932–6943
44. Kim TJ, Kim SK, Kim BJ, Son HJ, Hahn JS, Cheong M, Mitoraj M, Srebro M, Piękoś Ł, Michalak A, Kang SO (2010) Chem Eur J 16:5630–5644
45. Srebro M, Piękoś Ł, Kim TJ, Cheong M, Ok MA, Kang SO, Michalak A (2010) Macromol Res 18:960–966. doi:10.1007/s13233-010
46. Rossin A, Caporali M, Gonsalvi L, Guerri A, Lledós A, Peruzzini M, Zanobini F (2009) Eur J Inorg Chem 21:3055–3059
47. Charles W, Hamilton R, Baker T et al (2009) Chem Soc Rev 38:279–293
48. Parr RG, Ayers PW, Nalewajski RF (2005) J Phys Chem A 109:3957–3959
49. Baerends EJ, Autschbach J, Bashford D, Berger JA, Bérces A, Bickelhaupt FM, Bo C, de Boeij PL, Boerrigter PM, Cavallo L, Chong DP, Deng L, Dickson RM, Ellis DE, van Faassen M, Fan L, Fischer TH, Fonseca Guerra C, Giammona A, Ghysels A, van Gisbergen SJA, Götz AW, Groeneveld JA, Gritsenko OV, Grüning M, Harris FE, van den Hoek P, Jacob CR, Jacobsen H, Jensen L, Kadantsev ES, van Kessel G, Klooster R, Kootstra F, Krykunov MV, van Lenthe E, Louwen JN, McCormack DA, Michalak A, Mitoraj M, Neugebauer J, Nicu VP, Noodleman L, Osinga VP, Patchkovskii S, Philipsen PHT, Post D, Pye CC, Ravenek W, Rodriguez JI, Romaniello P, Ros P, Schipper PRT, Schreckenbach G, Seth M, Snijders JG, Solà M, Swart M, Swerhone D, te Velde G, Vernooijs P, Versluis L, Visscher L, Visser O, Wang F, Wesolowski TA, van Wezenbeek EM, Wiesenekker G, Wolff SK, Woo TK, Yakovlev AL, Ziegler T (2009) ADF 2009. 01; SCM: Amsterdam, The Netherlands
50. te Velde G, Bickelhaupt FM, Baerends EJ, Fonseca Guerra C, van Gisbergen SJA, Snijders JG, Ziegler T (2001) J Comput Chem 22:931–967, and references therein
51. Baerends EJ, Ellis DE, Ros P (1973) Chem Phys 2:41–51
52. Boerrigter PM (1988) te Velde G, Baerends EJ. Int J Quantum Chem 33:87–113
53. Fonesca Geurra C, Visser O, Snijders JG, te Velde G, Baerends EJ (1995) In: Clementi E, Corongiu G (eds) Methods and techniques in computational chemistry METACC-9.STEF, Cagliari, pp 303–395
54. Becke A (1988) Phys Rev A 38:3098–3100
55. Perdew JP (1986) Phys Rev B 34:7406–7406
56. ADF-GUI 2009.01, SCM, Amsterdam, The Netherlands, http://www.scm.com (Visser O, Leyronnas P, van Zeist WJ, Lupki M)
57. van Lenthe E, Baerends EJ, Snijders JG (1993) J Chem Phys 99:4597–4610
58. van Lenthe E, Baerends EJ, Snijders JG (1994) J Chem Phys 101:9783–9792
59. van Lenthe E, van Leeuwen R, Baerends EJ, Snijders JG (1996) Int J Quantum Chem 57:281–293
60. Kim SK, Han WS, Kim TJ, Kim TY, Nam SW, Mitoraj M, Piękoś Ł, Michalak A, Hwang SJ, Kang SO (2010) J Am Chem Soc 132:9954–9955
61. Fernàndez FM, Bickelhaupt MF, Cossion FP (2009) Chem Eur J 15:13022–13032
62. Rablen PR, Hartwig JF (1996) J Am Chem Soc 118:4648–4653